PERGAMON

International Journal of Heat and Mass Transfer 45 (2002) 4957–4966

International Journal of HEAT and MASS TRANSFER

www.elsevier.com/locate/ijhmt

Heat transfer enhancement from enclosed discrete components using pin–fin heat sinks

Enchao Yu [a], Yogendra Joshi [b,*]

[a] *OptoIC Technology, Inc., Irvine, CA 92620, USA*

[b] *G.W. Woodruff School of Mechanical Engineering, Georgia Institute of Technology, Atlanta, GA 30332, USA*

Received 31 May 2001; received in revised form 24 May 2002

Abstract

Computational modeling, temperature measurements, and flow visualizations were conducted to investigate the enhancement of combined natural convection, conduction, and radiation heat transfer from a 25.4 mm × 25.4 mm discrete heat source in a 127 mm × 127 mm and 41.3 mm high enclosure, using pin–fin heat sinks. The pin–fin array was attached to the heated component, which was flush mounted on the enclosure base. Effects of flow confinement by enclosure walls on heat transfer from the pin–fin heat sink were found prominent. The existing natural convection heat transfer correlations for pin–fin arrays in free space showed large deviations from present measurements. Radiation was also found to contribute significantly to the overall heat transfer. Experimental results show that enhancement of heat transfer using pin–fin heat sinks was significantly different for horizontally and vertically heated orientations of the enclosure.

Keywords: Heat transfer; Pin–fin heat sink; Natural convection; Radiation; Electronics cooling

1. Introduction

Fin arrays have been widely used in enhancing natural convection cooling of electronic packages. A recent detailed discussion on analysis and design of finned array heat sinks was presented by Kraus and Bar-Cohen [1]. While considerable information exists on plate fins [1,2], relatively less information on natural convection in pin–fin arrays is available. Sparrow and Vemuri [3,4] experimentally investigated natural convection and radiation heat transfer from arrays of pin fins with density in the range 0.31–1.33 pins/cm^2. The ratio of fin diameter to lateral fin spacing was found to play a significant role and its optimum value was found to be close to 0.5. The orientation effects of pin fins were also investigated and found to change the overall heat transfer by 15–20%. Radiation was found to be an important factor, contributing 25–45% of the overall heat transfer.

Zografos and Sunderland [5,6] reported on experimental and numerical studies on natural convection heat transfer from pin–fin arrays. They found an optimum ratio of 0.333 for a 203 × 203 square array of pin fins. In contrast to Sparrow and Vemuri [3], they found that the orientation of pin–fin arrays had a very limited effect on the heat transfer.

Aihara et al. [7] performed a detailed experimental investigation of natural convection and radiation heat transfer from pin–fin arrays with a vertical base plate. Totally, 59 types of circular pin–fin dissipaters were used. They employed a symmetrical geometry about a common base to minimize the heat loss from the base plate. Temperature measurements and flow visualizations were conducted and an empirical expression for the average heat transfer coefficient was derived.

Fisher and Torrance [8] presented an analytical solution for free convection limits for pin–fin cooling. The chimney effect was shown to enhance heat transfer.

* Corresponding author. Tel.: +1-40-4-385-2810; fax: +1-40-4-894-8496.

E-mail address: yogendra.joshi@me.gatech.edu (Y. Joshi).

0017-9310/02/$ - see front matter
PII: S0017-9310(02)00200-4

Nomenclature

A	heat transfer area (m^2)
A_b	base area of the pin–fin array (m^2)
Da	Darcy number, $Da = K/L_c^2$
F	view factor
g	gravitational acceleration (m/s^2)
G	irradiation (W/m^2)
h_{cp}	thickness of component (m)
H_w	thickness of enclosure wall (m)
H	height of enclosure (m)
h	heat transfer coefficient ($W/m^2\,K$)
J	radiosity (W/m^2)
k	thermal conductivity (W/m K)
K	permeability (m^2)
l_{cp}	length of component (m)
L	length of enclosure (m)
Nu	Nusselt number
p	pressure (N/m^2)
p_0	reference pressure (N/m^2)
Pr	Prandtl number
q''	heat flux (W/m^2)
Q	heat generation rate of the component (W)
Q_r	normalized radiative flux
Ra	Rayleigh number
R_b	ratio of case thermal conductivity to fluid thermal conductivity
R_{cp}	ratio of component thermal conductivity to fluid thermal conductivity
R_{en}	heat transfer enhancement factor
R_s	ratio of substrate thermal conductivity to fluid thermal conductivity
R_{ja}	junction-to-air thermal resistance (°C/W)
S_p	size of the pin (m)
S_{ps}	pin spacing (m)
S_v	ratio between opening area and the top wall area ($L \times L$)
T	temperature (K)
u, v, w	velocity in x, y, z directions respectively (m/s)
x, y, z	Cartesian coordinate (m)
U, V, W	non-dimensional velocity in x, y, z directions respectively
X, Y, Z	non-dimensional Cartesian coordinate

Greek symbols

α	thermal diffusivity of fluid (m^2/s)
β	coefficient of volumetric expansion (K^{-1})
ε	surface emissivity
δ	porosity
μ	dynamic viscosity ($N\,s/m^2$)
ν	kinematic viscosity (m^2/s)
θ	non-dimensional temperature
ρ	density of fluid (kg/m^3)

Subscripts

a	ambient
b	base plate
cond	conduction
cp	component
conv	convection
f	fluid
rad	radiation
p	pin fin
s	sink

They also demonstrated that the minimum thermal resistance for conventional heat sinks was about two times higher than the ideal limit based on inviscid flow with idealized local heat transfer.

Due to the densely populated pin fins in typical heat sinks, modeling each pin individually makes the numerical simulation of the entire heat sink nearly intractable compuatationally. Instead, the pin–fin arrays can be treated as a porous medium. A similar situation was encountered by Heindel et al. [9] who reported a study of enhancement of natural convection from an array of discrete heat sources in liquid filled enclosures. They used straight plate-fins to enhance heat transfer, and modeled them by treating the plate-fins as porous media. The predicted thermal resistances using a two-dimensional model followed the experimental trends.

In most applications, heat sinks are placed within enclosed spaces. In modern electronic products the emphasis is on making the enclosures more compact. The heat sink performance as a result is expected to be different from that measured in extensive surroundings. Heat sinks are often employed to provide thermal control to individual discrete heat sources or components. These heat sources are typically mounted on substrates such as printed wiring boards, and as a result conjugate conduction effects are usually significant. Increasingly, such heat sinks are being used as standard building blocks of electronic systems. With ever decreasing product development time, there is considerable interest in developing modeling approaches. All the studies of pin–fin heat sinks in the literature are experimental in nature. The present investigation was motivated by the preceding concerns.

In the present study, a pin–fin array heat sink was employed to study the combined conduction, natural convection and radiation in air cooled compact electronic enclosures motivated by thermal management of desktop power supply units. Both computations and supporting experiments were conducted for a vertically

heated enclosure configuration. The effects of radiation, fin density, and enclosure opening were also evaluated. Experiments were also performed on a horizontally heated enclosure to investigate the impact of orientation of the heat sink on natural convection cooling of a discrete heat source.

2. Enclosure geometry and experimental arrangement

In the present study, both vertically and horizontally heated enclosures were considered. The same experimental setup was used and the two orientations were achieved by rotating the enclosure by 90°. The configuration is seen in Fig. 1 and consists of two rectangular plexiglass enclosures. The external box was employed to simulate a well defined boundary condition, damp out stray circulations and thereby create a natural convection environment. A smoke inlet was mounted on the top of the external enclosure, which was sealed during temperature measurements. The internal box was of actual interest. The heat is removed from the internal enclosure through radiation and natural convection, and eventually removed from the external enclosure into ambient. In the present study, geometric parameters are chosen as defined in Table 1. Two values of the porosity of the pin–fin heat sink, as defined by the ratio of the

Table 1
Geometric parameters used in the present study

Enclosure		Pin–fin heat sink	
Parameter	Value (mm)*	Parameters	Value (mm)*
L	127	L_s	25.4
H	41.3	H_p	5.5
l_{cp}	25.4	H_b	1.75
h_{cp}	0.861	S_p	1.5
H_w	6.35	δ	0.5/0.72

* All except δ, which is dimensionless.

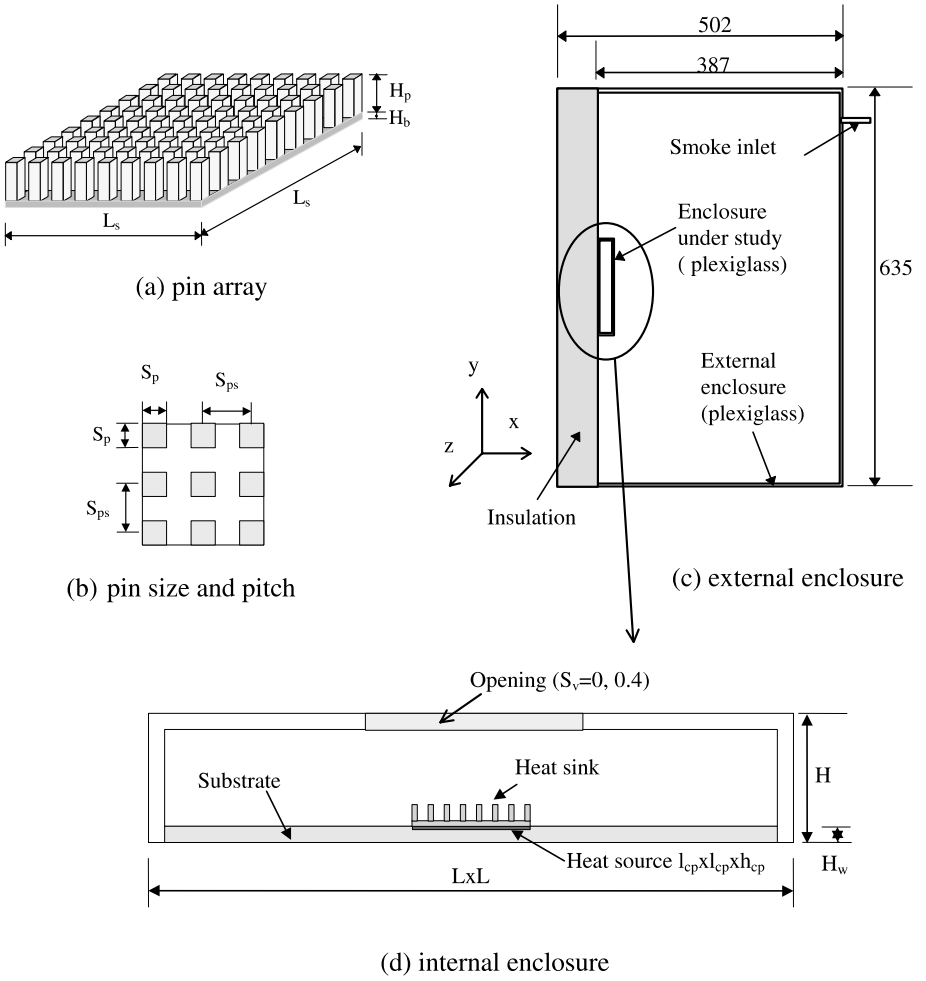

Fig. 1. Geometry of enclosures with pin–fin arrays on the heat source (all dimensions are in mm).

fluid volume to the total volume of the heat sink envelope, were chosen to be 0.5 and 0.72, corresponding to pin array sizes of 9×9 and 12×12 respectively. The fin material was aluminum.

A single thermofoil heater was flush mounted centrally on a plexiglass substrate. The pin–fin array was surface mounted on the heat source using 0.051 mm thick thermal conductive adhesive tape. The surfaces of the substrate and the pin–fin heat sink were painted black using Krylon 1602 of known surface emissivity of 0.95. Copper–constantan thermocouples of 0.076 mm diameter were employed for temperature measurements. Two thermocouples were attached to the heater bottom and four to the heat sink base. The ambient temperature was measured at the upper corner of the external enclosure. A data acquisition system (DAS) was used for temperature measurements. A personal computer based software written in Labview controlled the DAS by configuring the voltmeter for temperature measurements. The sampling frequency was also controlled by Labview. A general purpose interface bus (GPIB) card was used for managing the data transition between the computer and the DAS.

The temperature measuring system was calibrated using an ice-water bath and a precision mercury thermometer, with the resulting measurement uncertainty estimated as ± 0.1 °C. In the thermocouple placement, the uncertainty was estimated as ± 0.5 mm. Surface emissivity of plexiglass was quoted at an uncertainty of ± 0.01 and that of Krylon 1602 was ± 0.05 by the vendors. Uncertainties in voltage and current measurements are $\pm 0.4\%$ and $\pm 1.5\%$, respectively, resulting in an uncertainty of $\pm 1.6\%$ for the power input of 0.5 W, based on the uncertainty analysis method described by Kline and McClintock [10].

Flow visualizations were conducted using cigarette smoke illuminated with a 20 mW helium–neon laser sheet generated using a cylindrical lens. All the flow visualizations were performed at night to reduce the ambient interference. The time duration of the laser sheet was maintained less than 60 s to prevent radiative heating of the internal surfaces of the enclosure by the laser. The smoke generator was designed to produce smoke near ambient temperature, and a filter was employed to clean the smoke to reduce deposition of contaminants on the internal walls of the enclosures. Kodak TMAX 400 black & white films were employed to capture the flow patterns using a 35 mm Nikon F-3 camera. Exposure times ranged from 0.5 to 2 s, for different test conditions. Aperture settings were in the range 4–5.6.

3. Computational models and numerical method

Natural convection in the enclosure and within the heat sink, conduction in the component, base plate and substrate, and radiation interactions among different walls including the bounding surfaces of the heat sink and environment were solved in a combined fashion. Steady state laminar natural convection under the Boussinesq approximation was considered in the present study. The specific models for porous media transport for the heat sink and the radiation interactions are discussed next.

3.1. Porous media model for the heat sink

For natural convection in large porosity media, inertia effects can be significant, as reported by Heindel et al. [9] and Lauriat and Prasad [11]. Therefore, a Brinkman–Forchheimer model was used for the pin–fin array with the dispersion term neglected due to the small velocities in natural convection. Local thermal equilibrium was assumed between the air and the pin fins. The porous medium was considered homogeneous and with orthotropic thermal conductivity. The dimensionless governing equations for the entire domain including porous media, solid and air are as follows:

Continuity

$$\frac{\partial U_i}{\partial X_i} = 0 \tag{1}$$

Momentum

$$\frac{1}{\delta^2}\frac{\partial U_i U_j}{\partial X_i} = -\frac{\partial P}{\partial X_i} + \frac{1}{\delta}(Pr/Ra)^{1/2}\left(\frac{\partial^2 U_j}{\partial X_i \partial X_i}\right) + S_j \tag{2}$$

Energy

$$\frac{\partial (U_i \theta)}{\partial X_i} = \sum_{j=x,y,z}\left(\Gamma_j \frac{\partial^2 \theta}{\partial X_i \partial X_i}\right) + S_q \tag{3}$$

For the porous pin–fin array, the source term S_j is

$$S_x = -\frac{1}{Da}\left(\frac{Pr}{Ra}\right)^{1/2} U - \frac{C}{\sqrt{Da}}|\overline{V}|U \tag{4a}$$

$$S_y = -\frac{1}{Da}\left(\frac{Pr}{Ra}\right)^{1/2} V - \frac{C}{\sqrt{Da}}|\overline{V}|V + \theta \tag{4b}$$

$$S_z = -\frac{1}{Da}\left(\frac{Pr}{Ra}\right)^{1/2} W - \frac{C}{\sqrt{Da}}|\overline{V}|W \tag{4c}$$

and for air, S_j is

$$S_x = S_z = 0 \tag{5a}$$

$$S_y = \theta \tag{5b}$$

The diffusion coefficient is

$$\Gamma_j = \frac{k_j}{k_f}\frac{1}{(RaPr)^{1/2}}, \quad j = x, y, z \tag{6}$$

The energy source term S_q was zero except for the component where

$$S_q = -\frac{1}{H_{cp}}\left(\frac{1}{RaPr}\right)^{1/2} \tag{7}$$

The permeability K employed in Da was calculated based on the formula for flow across a bundle of cylinders suggested by Kaviany [12] using the following relation:

$$\frac{K}{d^2} = 0.0606\frac{\pi}{4}\frac{\delta^{5.1}}{1-\delta}, \quad 0.4 \leqslant \delta \leqslant 0.8 \tag{8}$$

where, d is the diameter of the pin fin and δ is the porosity. In the present study the hydraulic diameter was employed for the pin fins of a square cross-section.

The effective thermal conductivity components k_x, k_y and k_z of the porous medium, as described in Table 2, were determined using parallel and series resistance network models. We note that k_y and k_z had the same value and k_x was different. The coefficient C in Eqs. (4a)–(4c) was a constant and determined by the porous medium. In the present study C was fixed at 0.55, as suggested by Ward [13].

The normalization of parameters was implemented based on the characteristic length l_{cp} and the characteristic velocity $U_0 = (g\beta Q/k_f)^{1/2}$. The pressure and temperature were normalized respectively as $P = (p - p_0)/(\rho U_0^2)$ and $\theta = (T - T_a)/T_{ref}$ where $T_{ref} = Q/(l_{cp}k_f)$. The Rayleigh number was given by $Ra = g\beta Q l_{cp}^2/(\alpha\nu k_f)$.

3.2. Radiation model

Radiation was incorporated based on the radiosity/irradiation method [14]. The enclosure interior surfaces were assumed to be opaque, diffuse and gray. These surfaces were divided into smaller regions called zones, each assumed to be isothermal. Irradiation G_i and radiosity J_i on zone i were given respectively by

$$G_i = \sum_{j=1}^{N} F_{ij}J_j \tag{9}$$

and

$$J_i = \varepsilon_i\sigma T_i^4 + (1-\varepsilon_i)\sum_{j=1}^{N} F_{ij}J_j \tag{10}$$

The view factors F_{ij} between any two zones were obtained from Howell [15]. The radiosity J_i could then be solved from Eq. (10) and the net radiation rates were obtained.

Table 2
Effective thermal conductivity components in W/mK of the porous media for different porosity δ

δ	k_x	k_y	k_z
0.5	100	0.07	0.07
0.72	56	0.04	0.04

In the current study, the radiation exchange between the various pins of the heat sink and from individual pins to the enclosure surfaces were not solved due to the large number of fins. A simplified approach was employed to cope with this complexity. Radiation exchange between the heat sink and the enclosure walls was assumed to occur only from the imaginary bounding surfaces of the heat sink. Average temperatures of these surfaces were used in radiation calculations. Due to the nearly uniform temperature distribution on the pin fins and narrow spaces between them, radiation inside the pin array was assumed insignificant in comparison to the radiative heat transfer from the external surfaces of the heat sink.

3.3. Boundary conditions

Corresponding to the experimental setup for vertical enclosures, a half domain symmetric with respect to the mid x–y plane was employed for the computational modeling. The back of the substrate was considered adiabatic and no-slip was applied. The other four boundaries were subjected to ambient temperature and zero velocity components. The boundary conditions at dissimilar material interfaces are as follows.

$$R_i\left(\frac{\partial\theta}{\partial X_n}\right)_i = R_j\left(\frac{\partial\theta}{\partial X_n}\right)_j - \delta_{ij}Q_r \tag{11}$$

$$\theta_i = \theta_j \tag{12}$$

$$U = V = W = 0 \tag{13}$$

where, X_n was the coordinate normal to the surface and i, j refer to the two different materials (s, cp, b, f). Also, the normalized radiative flux $Q_r = (q_r'' L^2)/Q$, $R_s = k_s/k_f$, $R_{cp} = k_{cp}/k_f$, $R_b = k_b/k_f$, and $R_f = 1.0$. In Eq. (11) $\delta_{ij} = 1$ when i refers to solid and j to fluid, $\delta_{ij} = -1$ when i refers to fluid and j to solid, and $\delta_{ij} = 0$ when both i and j refer to solid materials.

3.4. Numerical method

SIMPLER algorithm detailed by Patankar [16] was used in the numerical calculations. The solution of coupled conduction, natural convection and radiation was obtained by incorporating radiative flux as a source term in the energy equation. Radiation from the pin–fin array was resolved by a source term in the first row of nodes surrounding the heat sink. Radiation fluxes were calculated at each iteration to prevent overshoot in temperature which may cause divergence of the solution. Before implementing SIMPLER algorithm, view factors among each pair of effective surfaces were computed using a self-contained subroutine. The surface temperatures from previous iterations were employed for calculating radiative fluxes. The temperature for each radiation zone was on area averages over the

convection control volumes which overlap with the radiation zone.

A non-uniform grid pattern was employed, with fine grids used to capture the flow characteristics in the vicinity of the solid–air interfaces. Grid testing for convection and radiation was carried out. Overall, the computations were performed using a non-uniform grid of $40 \times 58 \times 28$ for conduction and convection. For the radiation calculations, it was found that the arrangement of grids on the substrate dominated the accuracy of the results, leading to finer grids applied there. Totally, 68 effective zones were employed for radiation.

The numerical solution was considered to be converged at an iteration when the ratio of the maximum temperature change to the maximum temperature was within 1×10^{-5}, the ratio of the maximum velocity change and the maximum velocity was within 1×10^{-4}, and the residual of the energy equation for the whole domain was within 1%.

4. Validation of models and comparison with experiments

The developed computational models were validated against benchmark computational results and compared with experimental data obtained in the present study.

4.1. Validation against computational data

The pure natural convection model was validated for a box with opposite heated and cooled side walls. The results for maximum velocity and *Nu* were found to be within 2% and 1% respectively of those reported by Mallinson and de Vahl Davis [17]. The radiation model was validated against analytical calculations. The results for radiation heat rates from the present model by suppressing convection and conduction were within 1% of those from direct calculations. Radiation energy balance, reciprocity relations, summation of view factors to unity, and symmetric allocation of radiation rates were all achieved.

The porous media model was validated with the results reported by Beckermann and Viskanta [18]. The model problem was natural convection in a porous medium formed by a random packing of spherical glass beads in a vertical rectangular cavity with opposite vertical hot and cold walls. A very good agreement was found between the two studies. The difference in maximum temperature was within 1%.

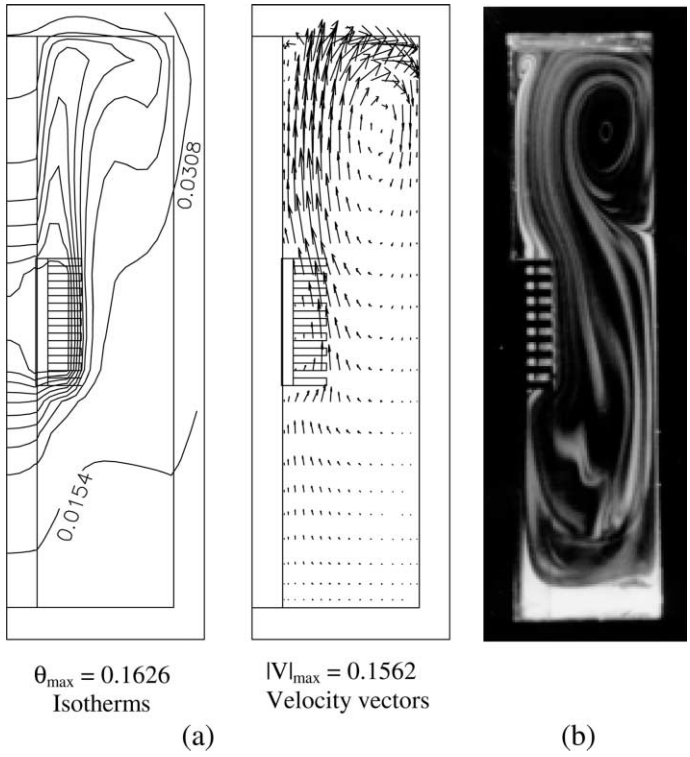

Fig. 2. Flow and temperature fields in the x–y plane at $z = 0$ in the vertically heated complete enclosure ($S_v = 0$) for $Ra = 2 \times 10^7$. Surface emissivity of the substrate and pin–fin array of porosity at 0.72 is 0.95 and the remaining surfaces are 0.83. (a) Computation, (b) flow visualization.

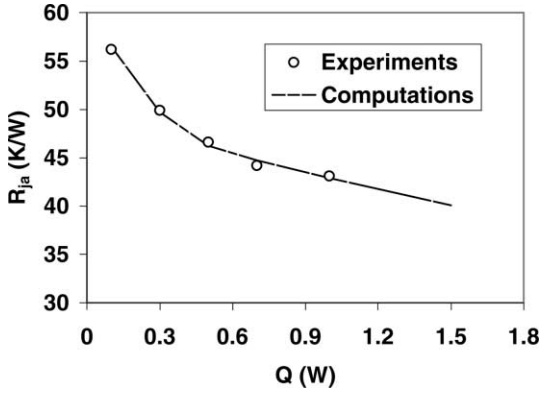

Fig. 3. Comparison of predicted and measured thermal resistances R_{ja} for different Q for the vertical complete enclosure.

4.2. Comparison with experimental data

The computationally obtained flow patterns for $Ra = 2 \times 10^7$ ($Q = 1.0$ W) are compared against the flow visualization in Fig. 2. It is seen that the model adequately predicts the flow patterns obtained in the visualizations. A strong flow recirculation was found in the upper corner and a nearly stagnant region in the lower part of the enclosure. We also see the flow passing through the pin–fin arrays. In comparison to the natural convection flow adjacent to the heat source without pin fins [19], a strong plume was seen right above the sink, and both thermal and flow regions were thickened, due to the heat spreading along the pins.

The computational results for the maximum temperature rise on the heat source in the form of thermal resistance were compared against experimental measurements. The thermal resistance of the discrete heat source was defined by

$$R_{ja} = (T_{\max} - T_a)/Q \tag{14}$$

This comparison in Fig. 3 shows the differences to be within 2%. These temperature measurements and flow visualizations provided further confidence in the computational modeling approach developed in the present study for the vertically heated configuration.

5. Heat transfer and flow characteristics

In this section, measurements are discussed for both vertically and horizontally heated enclosures. Computational predictions are presented only for vertically heated enclosures.

5.1. Heat transfer from pin–fin arrays

For multi-mode transport in compact enclosures, substrate conduction, natural convection and radiation have all been found to be significant (e.g. [3,19]). The total heat transfer rate is used to characterize the thermal performance of pin–fin heat sinks studied here. Fractions of the overall heat generation rate transferred by the three modes are also discussed. The non-dimensional parameters for presentation of computational results are as follows:

$$h = \frac{Q_s}{A_b(T_b - T_a)} \tag{15}$$

$$Nu = \frac{hL_s}{k_f} \tag{16}$$

$$Ra_T = g\beta(T_b - T_a)L_s^3/(\alpha^2 Pr) \tag{17}$$

where, Q_s is the total heat transfer rate from the heat sink side of the discrete component; A_b is the area of the heat sink base plate; T_b and T_a are respectively the temperatures at the base and the ambient. In all the computations, L_s, H, and S_p are fixed and only S_{ps} is varied for different porosities.

Fig. 4 displays the heat transfer characteristics as effective Nu for various Ra_T, and heat sink porosities.The data of Sparrow and Vemuri [3] and those for free convection along a vertical flat plate [20] of the same area as the heat sink base are also plotted in the same figure. It is observed that these results serve as the two limiting bounds for the present study. In comparison to the vertical flat plate, as expected, heat transfer is enhanced due to both heat sinking and radiation. It is, however, interesting to see the dramatic reduction in heat sink performance when it is placed within an enclosure. The effect of heat sink porosity observed in Fig. 4 is relatively minor in comparison. Nu at $\delta = 0.50$ is slightly less than that at $\delta = 0.72$, due to the reduced porosity weakening air flow through the fin spacings.

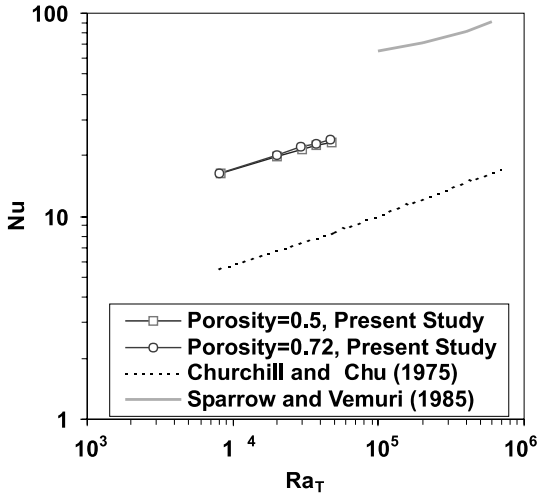

Fig. 4. Variations of effective Nu with Ra_T for different δ in the complete vertical enclosure (computation).

5.2. Relative importance of each heat transfer mode

The conjugate computations of the present study make it possible to evaluate the relative contributions of the three modes of thermal transport, which is difficult to achieve in a purely experimental investigation. It is known that heat spreading from discrete heat sources to substrates is a prominent effect in natural convection. Fig. 5 shows that 30–40% of heat is removed from the heat source through conduction in the substrate and the remaining is transferred through the pin–fin heat sink by convection and radiation. These ratios are strongly affected by the substrate thermal conductivity (e.g. [21]).

Heat lost through the heat sink by radiation is found to be in the range 40–55%. This fraction is slightly higher than the 40% reported by Sparrow and Vemuri [3], possibly resulting from the reduced convection component in the enclosed configuration studied here. Fig. 5 shows that radiation effect becomes more pronounced for lower *Ra* due to the reduced convection. The pin–fin array porosity δ is found to have a small effect on the fraction of heat transferred through various modes in the considered range.

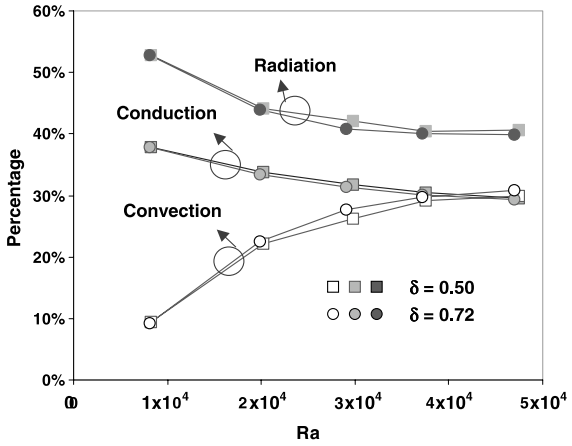

Fig. 5. Importance of the three heat-transfer modes for different δ in the vertical complete enclosures (computation).

5.3. Flow patterns for horizontal orientation

In horizontally heated enclosures, complex flows were formed. The general flow structures in the fin enhanced configuration are similar to those without pin–fin arrays. Strong center plume together with symmetric toroidal flows on each side are seen for both in Fig. 6(a) and (c). However, at the edges of the heat sink, see Fig. 6(b), two prominent flow cells were observed, induced by the fin array. These flow recirculations significantly enhance heat transfer from the heat source by increasing the heat exchange between the source and the top wall. When Q increases to 1.0 W as shown in Fig. 6(c) and (d), flow becomes more vigorous, due to increased buoyancy. No time dependent flows were observed in Fig. 6(c). However, when the heat sink was not employed, a strongly time dependent pulsating flow was observed in the experiments, as exhibited by the blurred image of the outer edge of the plume above the component in Fig. 6(d). The pin–fin arrays reduced the component temperature and stable flows were apparently attained as a result.

5.4. Heat transfer enhancement through enclosure opening

Partially open enclosures result in penetrative flows through the openings and may provide heat transfer enhancement. Additionally, in natural convection cooling applications the influence of orientation needs to be examined. Both effects are considered in the present

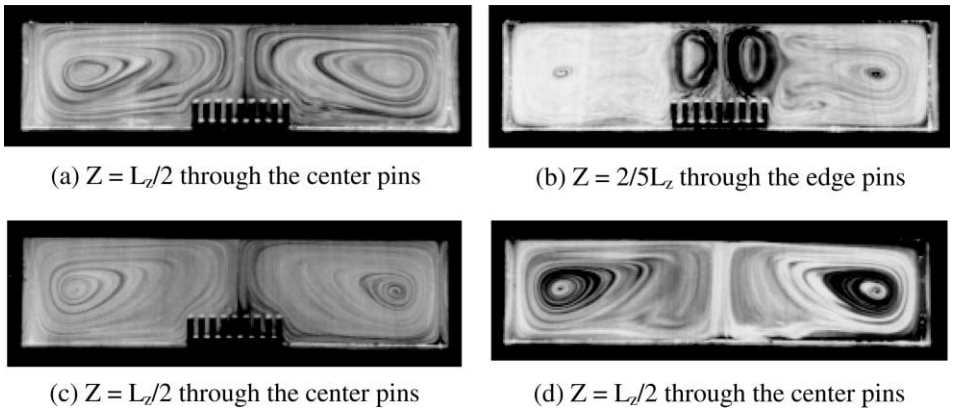

Fig. 6. Experimental flow visualizations in the selected x–y planes in horizontally heated complete enclosures with and without pin–fin arrays ($\delta = 0.72$) for variable Q. (a, b) $Q = 0.5$ W, (c, d) $Q = 1.0$ W.

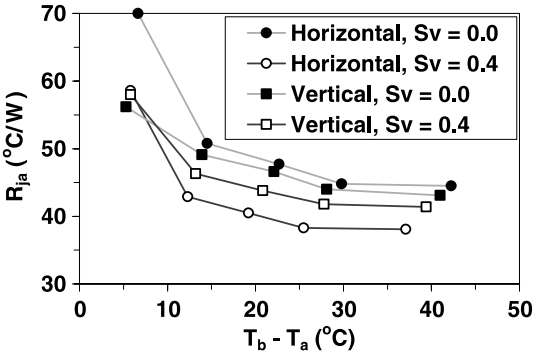

Fig. 7. Effect of enclosure orientation and opening on the thermal resistance of the discrete heat source using pin–fin heat sink ($\delta = 0.72$) (experiments).

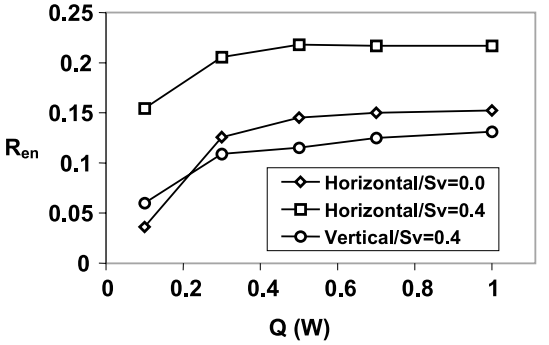

Fig. 8. Enhancement factor (R_{en}) of heat transfer for different Q by using pin–fin heat sinks of porosity at 0.72 for horizontal and vertical enclosures with and without openings.

experimental study in terms of thermal resistance defined in Eq. (15) and enhancement factor as defined by:

$$R_{en} = \frac{|R_{ja,s} - R_{ja}|}{R_{ja}} \tag{18}$$

where, $R_{ja,s}$ and R_{ja} are thermal resistances of the component with and without heat sinks respectively.

In Fig. 7, R_{ja} decreases with $T_b - T_a$ in general. The poorest thermal performance of the component is for a horizontal complete enclosure. It is also found that the smallest thermal resistance except for the smallest $T_b - T_a$, is for the horizontal box with opening on the top, instead of the vented vertical enclosure, indicating that vented horizontal enclosure in the presence of a pin–fin heat sink can be quite effective in heat transfer.

The effect of opening is found different for the two orientations in Fig. 7. The opening reduced R_{ja} by about 40% for the horizontal orientation, and <20% for the vertical enclosures. This is probably due to the less stable flows observed in visualizations for the horizontal configuration particularly for larger $T_b - T_a$. Different effects of orientation were found for closed and vented enclosures also in Fig. 7. For complete enclosures, the vertical orientation produces smaller thermal resistance, while the horizontal orientation results in better heat transfer for vented enclosures. The effects of opening on flow patterns have been described in the previous publications [19].

The enhancement factor R_{en}, is found to be dependent on the orientation and opening, see Fig. 8. The maximum decrease of R_{ja} is about 20% for $S_v = 0.4$ and 15% for $S_v = 0$ in horizontal enclosures. For vertical enclosures, the maximum decrease of R_{ja} is only 13% for $S_v = 0.4$, much lower than for horizontal enclosures. This finding is in general agreement with Sparrow and Vemuri [4]; however slightly higher enhancement of heat transfer (20%) in vented horizontal enclosures is obtained than that (15%) reported for a pin–fin array when the base plate is horizontal with fins pointing upwards. The observed flow cells in Fig. 6(b) might contribute to the enhanced heat transfer from the discrete heat source in comparison to the case without pin–fin heat sinks.

6. Conclusions

A porous media model was developed to simulate pin–fin heat sinks in vertical enclosures. Relative contributions of conduction, natural convection and radiation in the heat transfer enhancement from an enclosed discrete heat source using pin–fin heat sinks were studied. The enclosure walls provide shrouding and reduce the overall heat transfer compared to a heat sink in extensive ambient. However, thermal performance of the discrete heat source in such an enclosure was still better than without a pin array in free space. Overpopulated pin fins decreased the enhancement of heat transfer. Relative importance of various heat transfer modes was also examined and radiation was found to account for more than 40% of the overall heat transfer. Its contribution became even more significant for lower power levels.

Experiments showed substantial effects of opening and enclosure orientation. Presence of an opening reduced thermal resistance more prominently for horizontal enclosures than for vertical enclosures, by almost a factor of 2. For complete enclosures, vertical orientation produced lower thermal resistance. The enhancement of heat transfer from the discrete heat source using pin–fin arrays was found more significant for horizontal enclosures. Up to 20% reduction of the thermal resistance was attained when employing pin–fin heat sinks in the horizontal orientation with a 40% opening.

The flow visualizations in horizontal enclosures with pin fins revealed two explicit stable flow cells which were not seen in horizontal or vertical configurations without pin fins. The time dependent flow observed for

enclosures without a pin–fin array was replaced by a stable central plume when the pin–fin heat sink was employed.

Acknowledgements

This work was performed while the authors were with the University of Maryland, College Park. The authors would like to acknowledge the support of the Maryland Industrial Partnerships Program.

References

[1] A.D. Kraus, A. Bar-Cohen, Design and Analysis of Heat Sinks, John Wiley & Sons, New York, 1995.
[2] J Wei, K. Hijikata, T. Tomimura, M. Fujii, Numerical study on natural air cooling of fin arrays with enclosed boundaries, in: Advances in Electronic Packaging, INTERpack'97, Kohala Coast, Hawaii, EEP-vol. 19-2, 1997, pp. 2107–2114.
[3] E.M. Sparrow, S.B. Vemuri, Natural convection/radiation heat transfer from highly populated pin–fin arrays, J. Heat Transfer 107 (1985) 190–197.
[4] E.M. Sparrow, S.B. Vemuri, Orientation effects on natural convection/radiation pin–fin arrays, Int. J. Heat Mass Transfer 29 (1986) 359–368.
[5] A.I. Zografos, J.E. Sunderland, Natural convection from pin fins, Exp. Thermal Fluid Sci. 3 (1990) 440–449.
[6] A.I. Zografos, J.E. Sunderland, Numerical simulation of natural convection from pin–fin arrays, ASME HTD 157 (1990) 55–66.
[7] T. Aihara, S. Maruyama, S. Kobayakawa, Free convective/radiative heat transfer from pin–fin arrays with a vertical base plate (general representation of heat transfer performance), Int. J. Heat Mass Transfer 33 (6) (1990) 1223–1232.
[8] T.S. Fisher, K.E. Torrance, Free convection limits for pin–fin cooling, HTD-vol. 343, Proceedings of National Heat Transfer Conference, vol. 5, 1997, pp.129–138.
[9] T.J. Heindel, F.P. Incropera, S. Ramadhyani, Enhancement of natural convection heat transfer from an array of discrete heat sources, Int. J. Heat Mass Transfer 39 (3) (1996) 479–490.
[10] S.J. Kline, F.A. McClintock, Describing uncertainties in single-sample experiments, Mech. Eng. 75 (1953) 3–8.
[11] G. Lauriat, V. Parsad, Non-Darcian effects on natural convection in vertical porous enclosure, Int. J. Heat Mass Transfer 32 (1989) 2135–2148.
[12] M. Kaviany, in: Principles of heat transfer in porous media, second ed., Springer-Verlag, New York, 1991, p. 43.
[13] J.C. Ward, Turbulent flow in porous media, J. Hydraul. Div. ASCE 90 (1964) 1–12.
[14] F.P. Incropera, D.P. De Witt, in: Fundamentals of Heat and Mass Transfer, second ed., John Wiley & Sons, New York, 1990, pp. 639–642.
[15] J.R. Howell, in: A Catalog of Radiation Configuration Factors, McGraw-Hill, New York, 1982, pp. 96–99.
[16] S.V. Patankar, Numerical Heat Transfer and Fluid Flow, Hemisphere and McGraw-Hill, New York, 1980.
[17] G.D. Mallinson, G. de Vahl Davis, Three-dimensional natural convection in a box, a numerical study, J. Fluid Mech. 83 (1977) 1–31.
[18] C. Beckermann, R. Viskanta, Natural convection solid/liquid phase change in porous media, Int. J. Heat Mass Transfer 31 (1) (1988) 35–46.
[19] E. Yu, Y.K. Joshi, Heat transfer in discretely heated side-vented compact enclosures by combined conduction, natural convection, and radiation, J. Heat Transfer, Trans. ASME 121 (1999) 1002–1010.
[20] S.W. Churchill, H.H.-S. Chu, Correlating equations for laminar and turbulent free convection from a vertical plate, Int. J. Heat Mass Transfer 18 (1975) 1323.
[21] E. Yu, Y.K. Joshi, Effects of orthotropic thermal conductivity of substrates in natural convection cooling of discrete heat sources, Numer. Heat Transfer, Part A 32 (1997) 575–593.